Supporting Information

Second-Harmonic Generation and Photoluminescence Properties of Colloidal WS_2 Monolayers deposited from Solution

Yang Zhao[a,b‡], Markus Fröhlich[a‡], Marco Kögel[c], Onno Strolka[a,d,e], André Niebur[d,e], Tim Parker[a,b], Felix Schneider[a,b], Alfred J. Meixner[a,b], Jannik C. Meyer[c,f], Dai Zhang[a, b]*, Jannika Lauth[a,b,d,e]*

a) Institute for Physical and Theoretical Chemistry, Eberhard Karls University of Tübingen, Auf der Morgenstelle 18, 72076 Tübingen, Germany

b) Center for Light-Matter-Interaction, Sensors, and Analytics (LISA+), Eberhard Karls University of Tübingen, Auf der Morgenstelle 15, 72076 Tübingen, Germany

c) NMI Natural and Medical Sciences Institute at the University of Tübingen, Markwiesenstraße 55, D-72770 Reutlingen, Germany

d) Institute for Physical Chemistry and Electrochemistry, Leibniz University Hannover, Callinstr. 3A, D-30167 Hannover, Germany.

e) Cluster of Excellence PhoenixD (Photonics, Optics, and Engineering – Innovation Across Disciplines), Welfengarten 1A, D-30167 Hannover, Germany.

f) Institute of Applied Physics, Eberhard Karls University of Tübingen, Auf der Morgenstelle 10, D-72076 Tübingen, Germany

Corresponding Authors

*E-mail: dai.zhang@uni-tuebingen.de

*E-mail: jannika.lauth@uni-tuebingen.de

Supplementary Notes

A. Materials

Oleylamine (OlAm, 98 %), sulfur (99.98 %) oleic acid (OA, >99 %), hexane (HPLC grade) and ethanol (p.a.) were acquired from Sigma-Aldrich. Tungsten (VI) chloride (WCl_6, 99 %) was purchased from Alfa Aesar and 1,1,1,3,3,3-hexamethyldisilazane (HMDS, 98 %) was purchased from Acros Organics. All chemicals except for OlAm, hexane and ethanol were degassed, stored in the glovebox and used without further purification.

B. Methods

Purification of OlAm. Commercial OlAm (500 mL, pale yellow liquid) was dried under inert gas atmosphere over a 2 cm^3 piece of sodium at 200 °C for 2h. After cooling to room temperature, an oil pump vacuum was applied carefully and the OlAm was distilled at ~200 °C. The purified clear and colorless liquid was stored inside a nitrogen filled glovebox.

Synthesis of colloidal WS_2 NSs. For the preparation of the tungsten precursor, WCl_6 (3.75 mg, 9.5 μmol) is dissolved in OlAm (10 mL) inside a glovebox. Under inert atmosphere, elemental sulfur (2 mg, 62.4 μmol), OlAm (55 ml) and HMDS (0.65 ml, 3.1 mmol) are mixed in a three-neck flask and heated to 320 °C. The tungsten precursor is then added dropwise (10 ml/h) to the sulfur, OlAm and HMDS solution. The reaction mixture is stirred subsequently for an additional hour at 320 °C before allowing cooling to room temperature. The crude reaction product is precipitated by adding ethanol (100 mL) under ambient conditions. The precipitate is washed twice by redispersion in hexane (40 mL) and subsequent precipitation. Finally the WS_2 NSs are dissolved in 1,2-dichlorobenzene for increased colloidal stability.[1]

Preparation of samples for optical measurements. 3 μL of a precipitated and redispersed WS_2 solution were dropped onto a silicon wafer substrate and excess solvent was evaporated under vacuum. For further purification, a batch of the dried sample was washed

carefully by consecutively submerging in hexane and isopropanol until no residual OlAm (forming a waxy layer on the wafer), was observed.

Scanning electron microscopy. The morphology of 2D WS_2 was studied by scanning electronic microscopy (SEM, SU8030, Hitachi) under 1.0 kV applied acceleration voltage.

Transmission electron microscopy. TEM images were collected using a JEOL ARM 200F equipped with a CETCOR aberration corrector operating at 80 kV. Samples were prepared by drop-casting the colloidal WS_2 NS solution onto graphene-coated MEMS (Graphenea easy-transfer) heating chips purchased from Hennyz Solutions. The dry sample was cleaned according to the procedure described above and annealed at 150 °C overnight in the high vacuum of the electron microscope to remove mobile carbon contaminations.

PL/SHG measurement. For the linear optical measurements, a custom-built confocal microscope (Figure S3) with a parabolic mirror (PM) as the laser focusing and signal collection element was used. The microscope is equipped with a 532 nm CW laser (NANO 250-532 max, QIOPTIQ) for optical excitation. A mode converter consisting of four quarters of half-wave plates and a pinhole convert the linearly polarized laser beam to a radially or azimuthally polarized beam. An avalanche photodiode (APD, SPCM-AQR-14, Perkin Elmer) collects PL signals for optical imaging. To obtain optical spectra, a spectrometer coupled with a liquid nitrogen-cooled (CCD) camera (Acton Research, SpectraPro 300i, Perkin Elmer) is employed. For the nonlinear optical measurements,

another PM-assisted custom-built confocal optical microscope is used, which is equipped with a femtosecond pulsed laser source (pro NIR_02508, Toptica Photonic) with a central excitation wavelength of 779 nm (repetition frequency 40 MHz, pulse duration 89.8 fs). For these measurements, we used parabolic mirrors with numerical apertures (NA) of 0.998 in air for light focusing and collection. The SHG signals are spectrally selected with a 390 nm bandpass filter with a transmission window of ± 10 nm and detected by a single photon counting module (COUNT-100B, Laser Components). A spectrometer coupled with a thermoelectrically cooled CCD camera (Acton SP2500, Princeton Instruments) was used to record the optical spectra.

Fluorescence Lifetime Imaging (FLIM) with phasor plots. FLIM measurements including corresponding phasor plot analysis were carried out with a multimodal 5D multiphoton-laser system (Jenlab GmbH, Jena, Germany). The system is equipped with a femtosecond near-infrared Ti:sapphire laser (repetition frequency 80 MHz, pulse duration ≤ 100 fs, MaiTai, Spectra-Physics) which is tunable from 710 nm to 929 nm. In this work, a laser excitation with an output power 5 mW at a wavelength of 750 nm was used. An oil-immersion objective lens of NA 1.40 was used for focusing the laser and collecting the optical signal from the sample. For FLIM measurements, a time-correlated single photon counting (TCSPC) module (Becker & Hickl GmbH, Berlin, Germany) was applied. FLIM images were processed to perform a phasor plot analysis and calculate and export

fluorescence decay parameters with the SPCImage v8.5 software. (Becker & Hickl GmbH, Berlin, Germany).

Principle of FLIM calculation method (MEDF) and phasor plot approach (PPA). FLIM measurements collect the intensities, decay times (lifetimes τ) and corresponding distribution of emission signals, and the fluorescence lifetimes can be easily spectrally recorded with the TCSPC module. The schematic diagram of TCSPC detection channels in Figure 6a shows how the TCSPC system converts and masks photon signal into four parts from ultra-violet to visible band. Corresponding lifetimes of components τ_n and contributions α_n are modelled and calculated with conventional MEDF method as shown below:

$$\mathrm{I(t)} = \sum_{i=1}^{n} \alpha_n \exp\left(-\frac{t}{\tau_n}\right) + C \qquad \text{(S1)}$$

where I(t) is the intensity of photons at time t and C is offset (e.g. scattering effect, surrounding light and background noise). As mentioned above, the calculating accuracy of MEDF method relies on pre-selected parameters such as the number of involved components and chi-square iterations. To improve the fluorescence lifetime fitting quality, we introduced PPA to reach this goal since there are two advantages including the reduction of initial assumptions of the components contributing to fluorescence decay traces and no dependency on iterative calculations.[2] The main purpose of using PPA is to visualize the

lifetime distribution from different fluorescent components through the spatial dimension transformation. The TCSPC system's periodic signal from a pulsed femtosecond laser allows for the conversion of component lifetimes in a selected region using the Fourier transform, which can be expressed with:

$$\mathrm{R}(\omega) = \int_0^\infty I(t) \cdot e^{-i\omega t} dt \tag{S2}$$

Then the calculation result can be further separated into real and complex parts in order to analyze the contribution lifetimes from all components included in region:

$$\mathrm{G}_{m,n} = Re\big(R_{m,n}\big) = \frac{\int_0^\infty I_{m,n}(t)\cos(\omega t)\,dt}{\int_0^\infty I_{m,n}(t)\,dt} \tag{S3}$$

$$\mathrm{S}_{m,n} = Im\big(R_{m,n}\big) = \frac{\int_0^\infty I_{m,n}(t)\sin(\omega t)\,dt}{\int_0^\infty I_{m,n}(t)\,dt} \tag{S4}$$

where G and S are the spatial dimensions in phasor plot, Re and Im are the real and imaginary parts of components in Fourier transform respectively, and m, n are indices for row and column of input images. It is possible to determine the contribution lifetimes (τ_1 and τ_2) by finding the intersections of the fitted linear function with the universal circle and establishing the relationship between dimensions and lifetimes:

$$\mathrm{G} = \sum_{i=1}^{n} \alpha_i \cdot \frac{1}{1+\omega^2\tau_i^2} \tag{S5}$$

$$S = \sum_{i=1}^{n} \alpha_i \cdot \frac{\omega\tau_i}{1+\omega^2\tau_i^2} \quad \text{(S6)}$$

Meanwhile, the amplitude of the spots which are located inside the universal circle can be calculated by equations shown below:

$$\alpha = \sqrt{G^2 + S^2} \quad \text{(S7)}$$

$$\varphi = \arctan\left(\frac{S}{G}\right) \quad \text{(S8)}$$

In addition, the contribution from one component to the mixture can be determined by measuring the distances between the phasor M and the phasors from components 1 and 2 through $\frac{\beta_i}{\beta_1+\beta_2}$, this allows us to make further progress on quantitative analysis.

The purity of the sample can be confirmed by PPA through identifying the fluorescent features of chemical components. Figure S3a and S3b shows the lifetime distribution of unpurified and purified WS_2 NSs, there are two concentrated oval areas visible. A short lifetime, which corresponds to the WS_2 NSs and relatively long lifetime, corresponding to chemical residuals on the unpurified sample, while only the latter appears in the purified WS_2 NSs. The result reveals that PPA can be used as an effective method for colloidal TMDCs purity identification and the purity does play an important role in colloidal sample preparation. In addition, due to the setup time resolution (0.25 ns), the exact τ value of colloidal WS_2 NSs cannot be measured.

Nonlinear susceptibility applied formulas.

$$\frac{P_{SHGmax}(\omega_{WS_2-Flake})}{P_1^2(\omega_{WS_2-Flake})} = \frac{16\sqrt{2}S\omega^2}{c^3\varepsilon_0 f\pi r^2 t_{FWHM}(1+n_2)^6}\left|\chi^{(2)}_{s-WS_2-Flake}\right|^2 = k_1\left|\chi^{(2)}_{s-WS_2-Flake}\right|^2 \quad (S9)$$

$$\frac{P_{SHGmax}(\omega_{WS_2-Nanosheets})}{P_1^2(\omega_{WS_2-Nanosheets})} = \frac{16\sqrt{2}S\omega^2}{c^3\varepsilon_0 f\pi r^2 t_{FWHM}(1+n_2)^6}\left|\chi^{(2)}_{s-WS_2-Nanosheets}\right|^2 = k_2\left|\chi^{(2)}_{s-WS_2-Nanosheets}\right|^2 \quad (S10)$$

Since the k_1 and k_2 can be regarded as the calibration factors in the experiments, and the WS_2 samples were both measured on the same microscopy setup, k_1 is approximately equal to k_2. and the SHG intensity is proportional to the SHG power, we have $k_1 \approx k_2$. Then the slopes from colloidal and flake WS_2 samples can be calculated through the equation below:

$$\frac{Slope_{WS_2-Nanosheets}}{Slope_{WS_2-Flakes}} = \frac{\frac{I_{SHGmax}(2\omega_{WS2-Nanosheets})}{P_1^2(\omega_{WS2-Nanosheets})}}{\frac{I_{SHGmax}(2\omega_{WS2-Flakes})}{P_1^2(\omega_{WS2-Flakes})}} = \frac{\left|\chi^{(2)}_{s-WS2-Nanosheets}\right|^2}{\left|\chi^{(2)}_{s-WS2-Flake}\right|^2} \quad (S11)$$

Calculation of excitation power density using the Airy-disk model and a Gaussian beam distribution

The peak (I_{peak}) and average power densities (I_{avg}) are calculated for evaluating the damage threshold of 2PPL-SHG related nonlinear optical properties. Considering the Gaussian distribution of the femtosecond laser beam with the standard Rayleigh diffraction limit condition (Airy-disk model) in this work, the peak and average power densities can be

calculated by following equations:

$$r_f = \frac{0.61\lambda}{NA} \tag{S12}$$

$$A_f = \pi {r_f}^2 \tag{S13}$$

$$I_{avg} = \frac{P_f}{A_f} \tag{S14}$$

$$I_{peak} = \frac{P_f}{\omega_l T_{pulse} A_f} \tag{S15}$$

where r_f the effective radius of Airy-disk pattern at focus, A_f the effective focus area, ω_l the repetition frequency of femtosecond laser and T_{pulse} the effective pulse width under standard Gaussian distribution. The calculated peak power density values under 0.8 mW and 8 mW in nonlinear optical measurement are 52.1 GW/cm^2 and 521 GW/cm^2, respectively.

Supplementary Figures and Tables

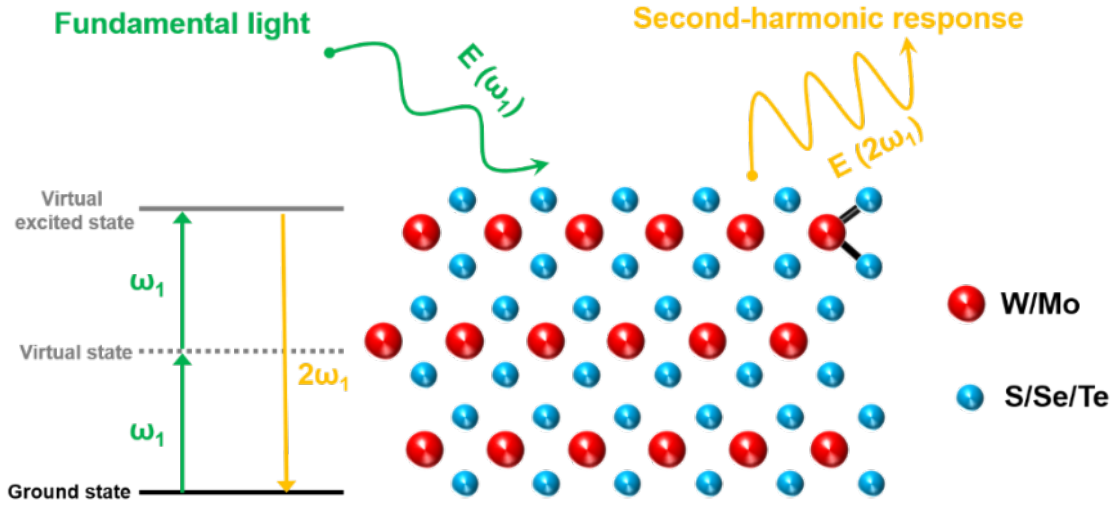

Figure S1. Schematic diagram of the second-harmonic generation process in layered TMDC materials.

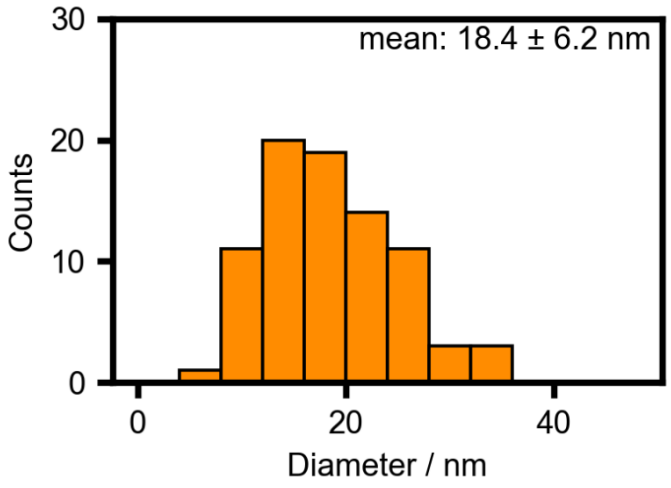

Figure S2. Size distribution of WS_2 NSs from TEM images.

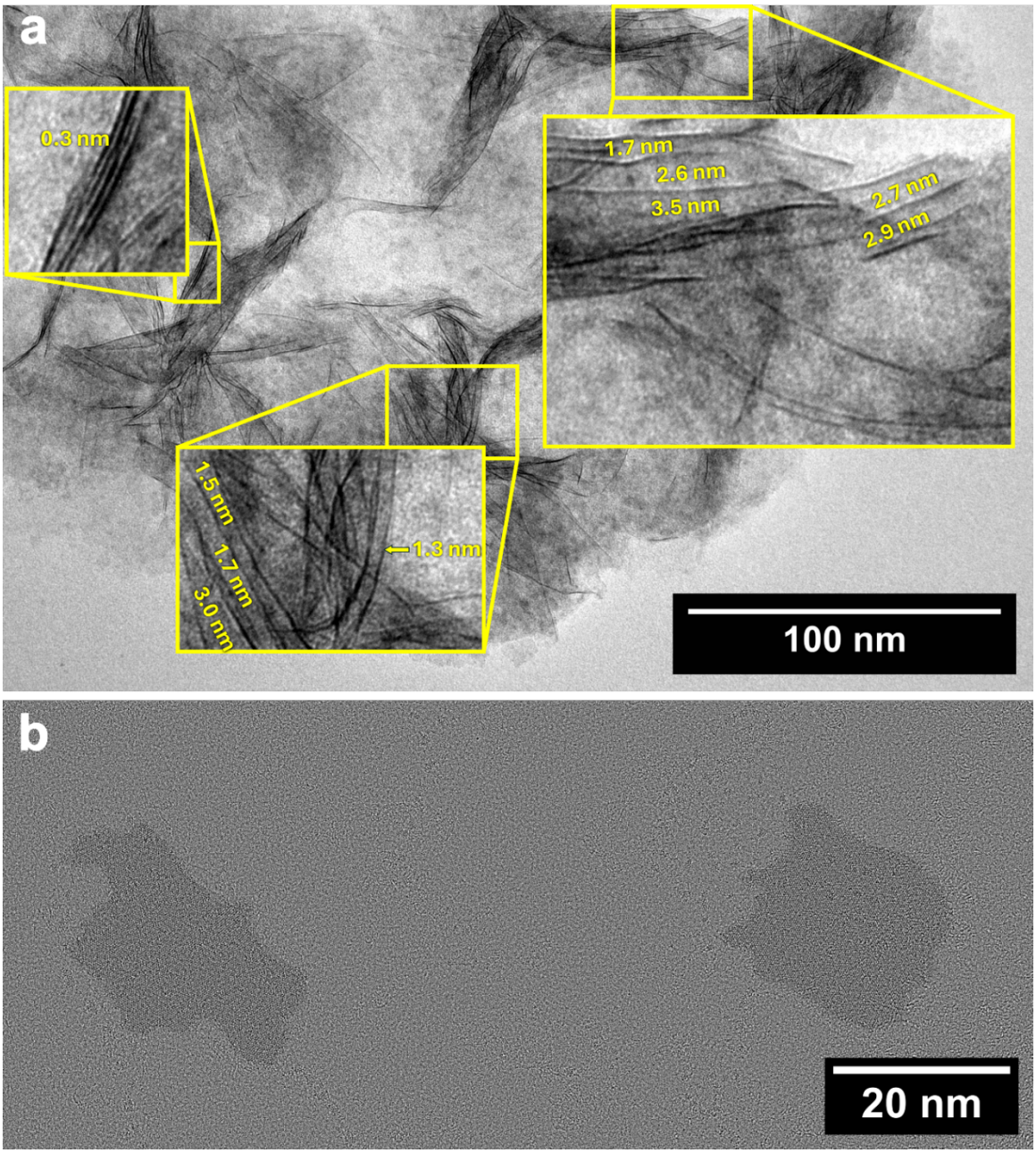

Figure S3. a) Low resolution TEM image of WS_2 nanoflower showcasing ligand-separated monolayers in the agglomerated state.b) High resolution TEM image of two individual flat lying WS_2 NSs as used for determining the lateral size.

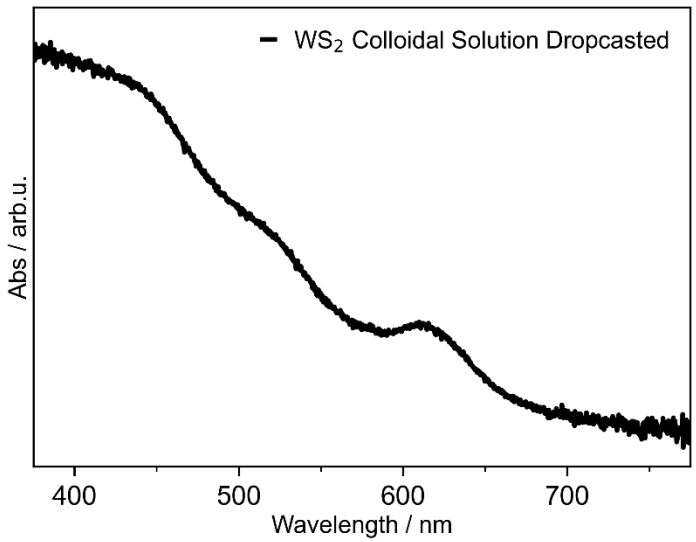

Figure S4. Absorbance spectrum of WS_2 NSs drop-casted from colloidal solution as prepared for the linear and nonlinear spectroscopy.

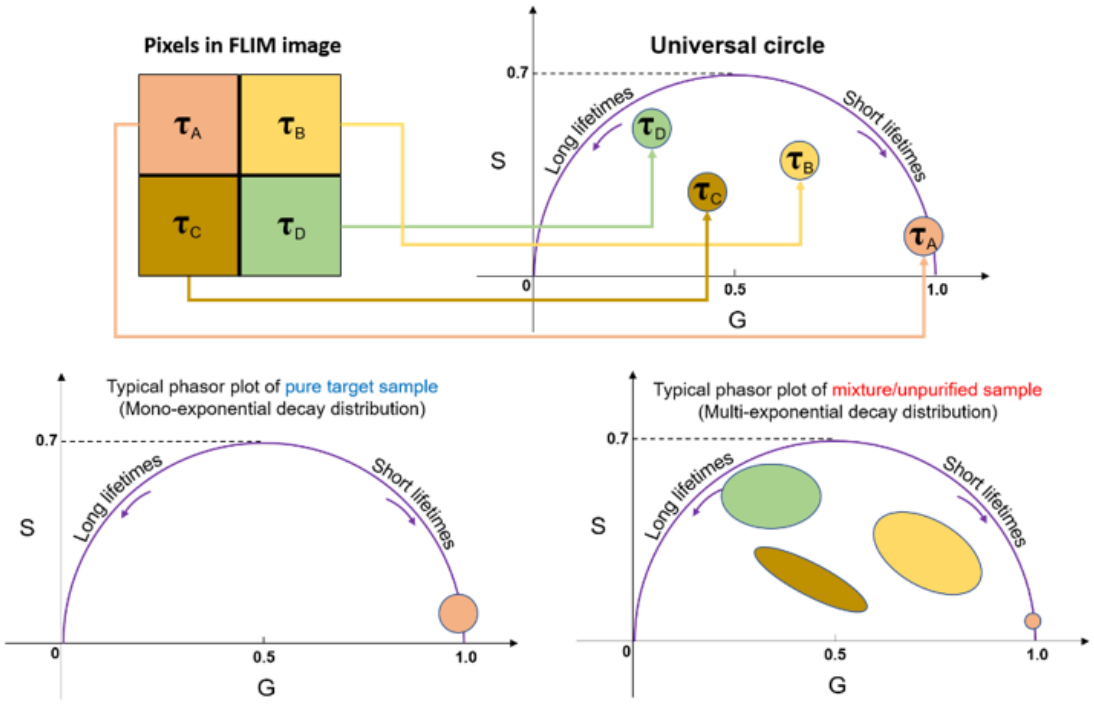

Figure S5. The schematic diagram illustrates a FLIM phasor analysis example with four ellipses, each representing a different lifetime (τ1 to τ4. Different fluorophores with distinct lifetimes can be discriminated by its species associated precise phasor. Using the geometrical working principle at the basis of the phasor-plot, different lifetime values (a cloud of points or lifetime cluster) are distributed over a semicircle where the "longest" lifetime are on the left side, while the "shortest" ones on the right side of the plot. A pure fluorescent sample without any residuals could show a certain lifetime value on the semi-circle, which fits the mono-exponential decay very well. On the contrary, an unpurified sample shows multiple lifetime clusters in the semi-circle, giving a multi-exponential decay. Through such changes on the phasor plot, the purity identification can be processed as a qualitative analysis.

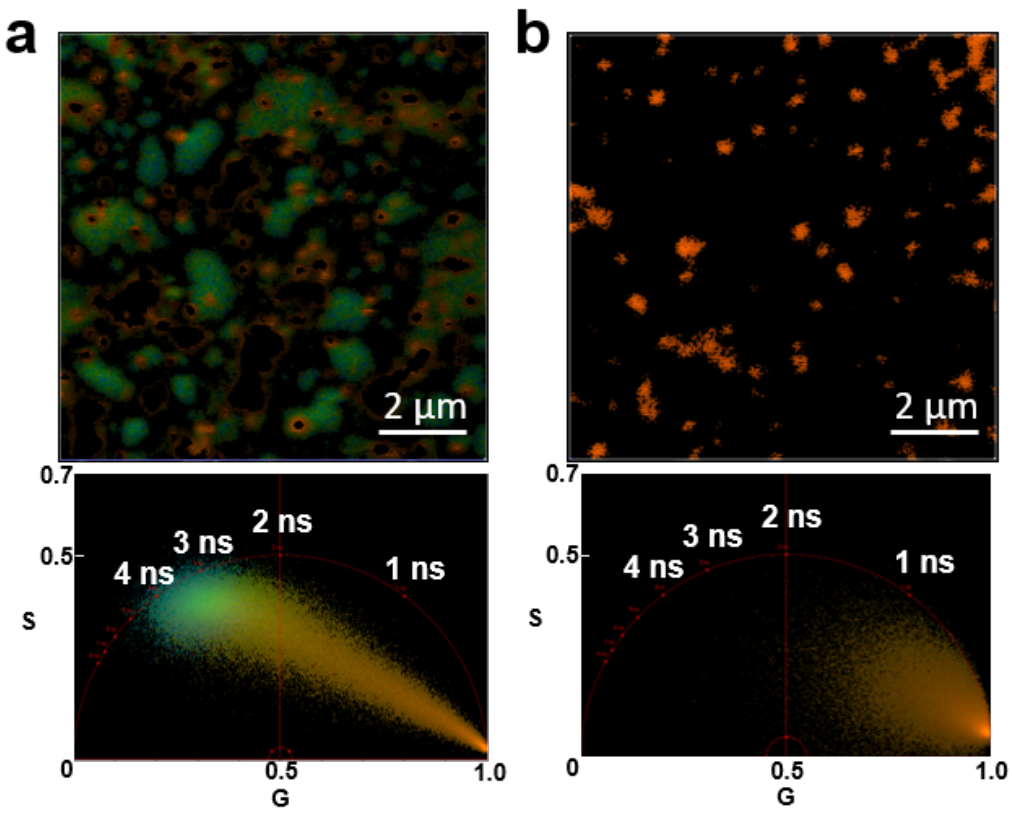

Figure S6. a) Distributed fluorescence lifetime image with corresponding phasor plot of unpurified WS_2 NSs, with spatial dimensions G and S from equation S5 and S6. b) Distributed fluorescence lifetime image with corresponding phasor plot of subsequently washed WS_2 NSs used for the description in the main manuscript. Vanishing of the long lifetime component in b) confirms the additional washing step to successfully remove residual OlAm.

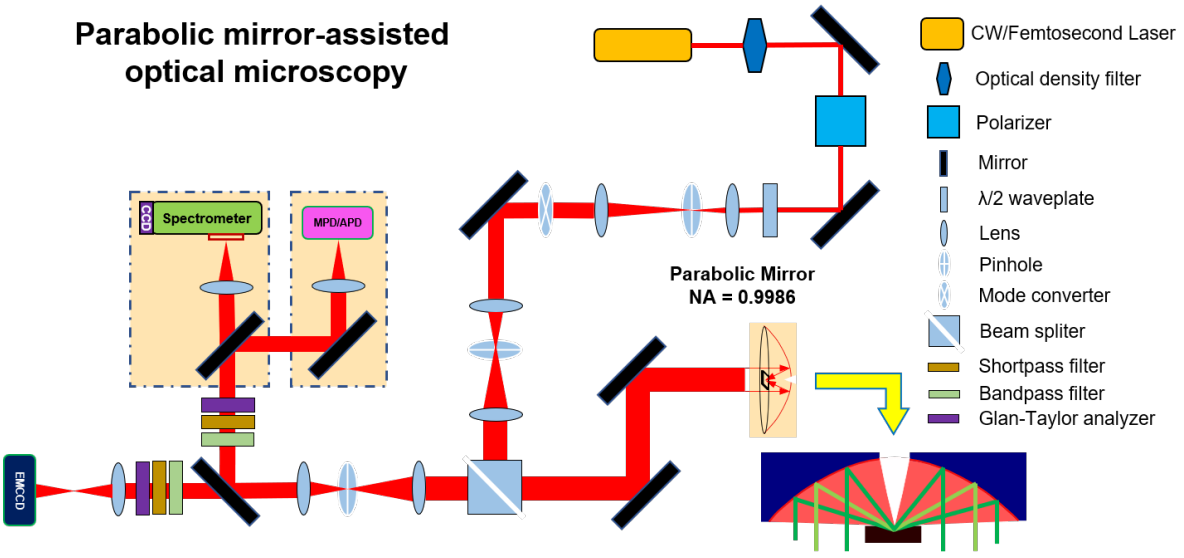

Figure S7. Schematic diagram of the home-built PM-assisted confocal microscopy setup.

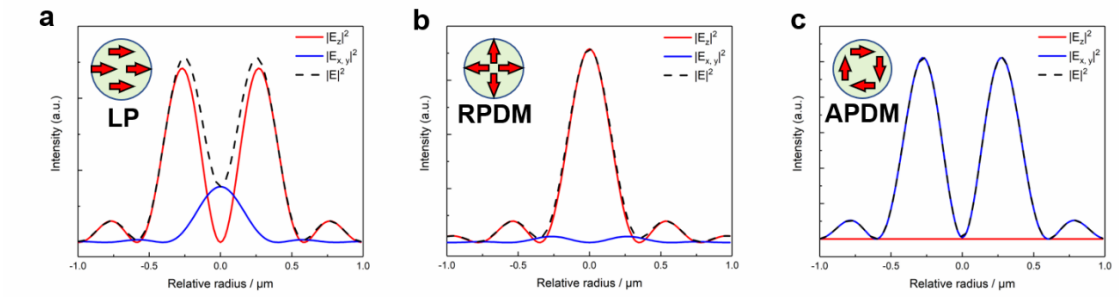

Figure S8. a), b), and c) Electric field intensity distribution under linear, radial and azimuthal polarization modes. The LP focal field contains intensities from E_z and $E_{x,y}$, the RPDM provides high E_z intensity, while APDM has only transverse $E_{x,y}$ intensity parallel to the substrate surface.

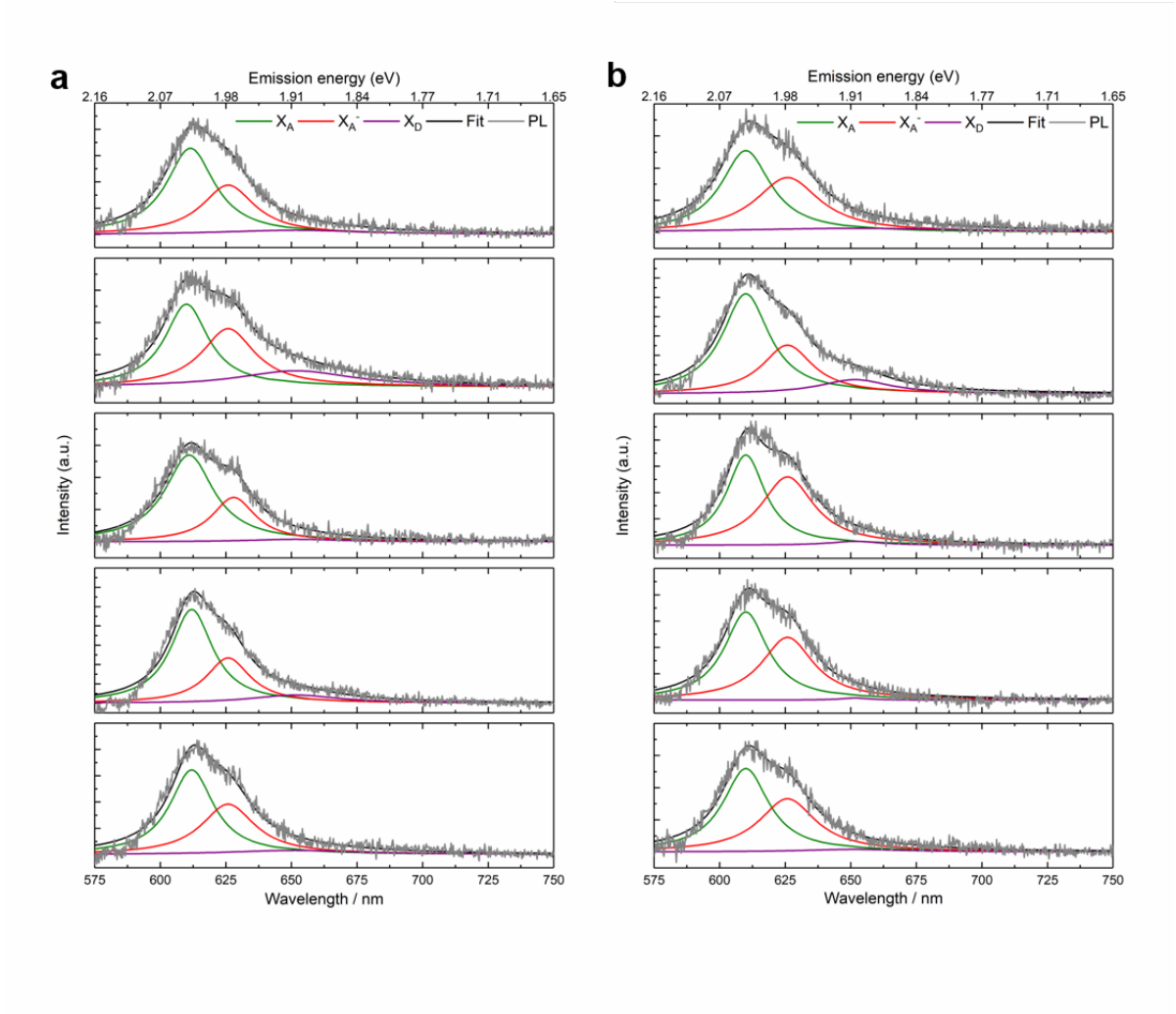

Figure S9. a) Fitted PL spectra collected from different spots under RPDM and b) APDM. The neutral exciton emission is the dominant signal and shows no dependence on laser polarization.

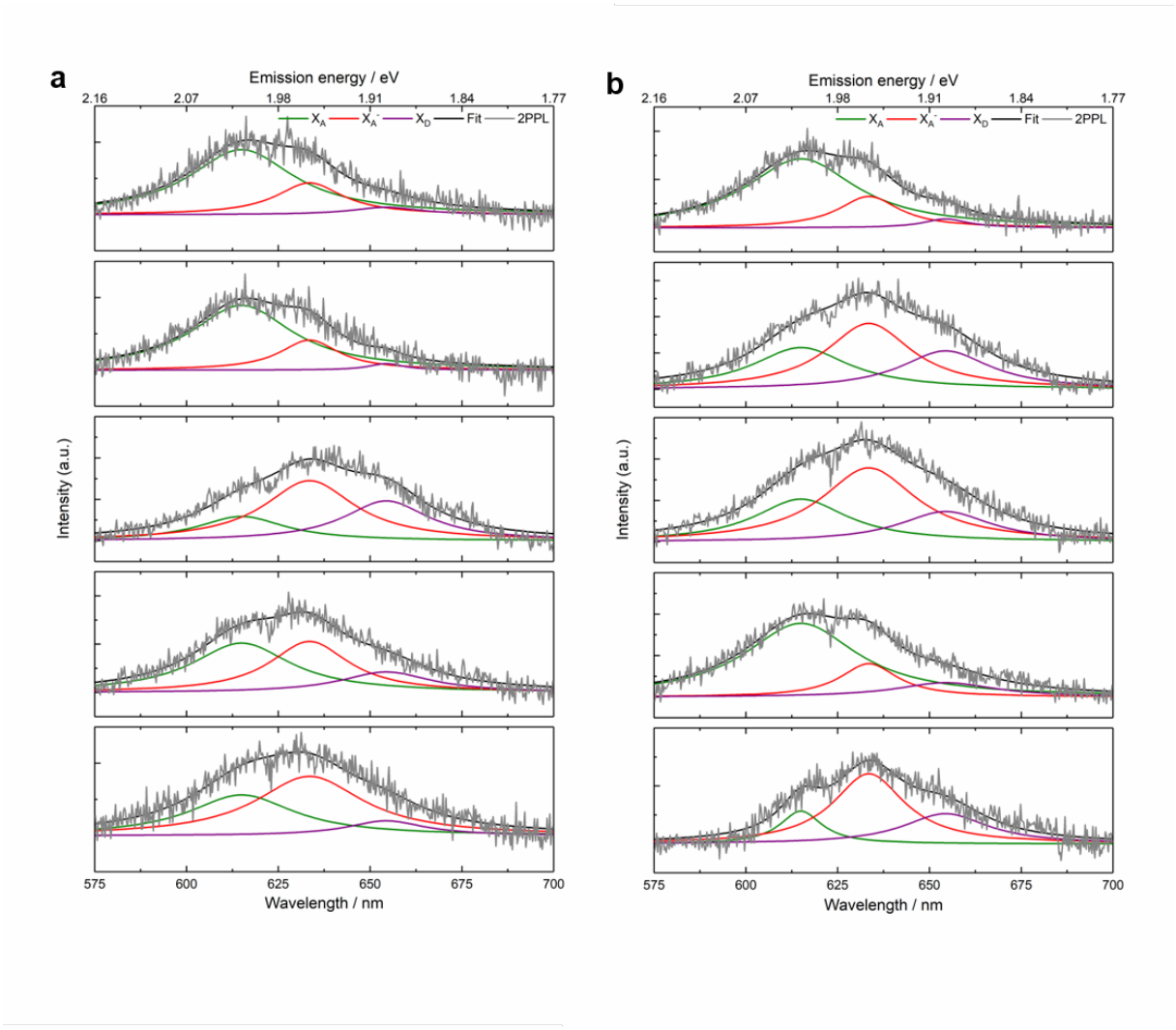

Figure S10. a) Fitted 2PPL spectra collected from different spots under RPDM and b) APDM. While the contribution to the 2PPL may vary from spot to spot, trion emission dominates the exciton emission in most cases.

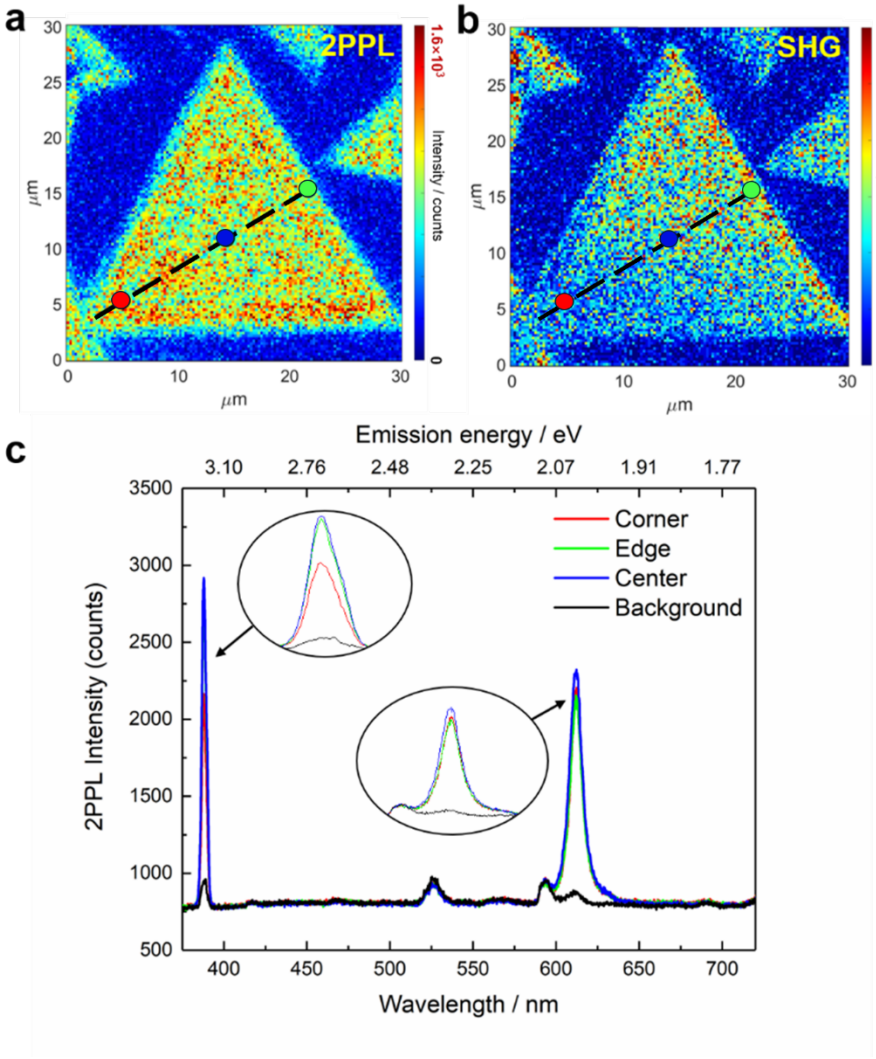

Figure S11. 2PPL and SHG intensity distribution and corresponding spectra of a CVD grown WS_2 flake. a) 2PPL intensity distribution of a CVD grown WS_2 flake; b) SHG intensity distribution image of CVD grown monolayer WS_2 flake; c) 2PPL spectra of a CVD grown WS_2 flake, collected at the spots shown in Figure S9a.

REFERENCES

1. P. Schiettecatte, S. Singh, P. Zhou and Z. Hens, *Langmuir*, 2023, **39**, 6568-6579.

2. M. Štefl, N. G. James, J. A. Ross and D. M. Jameson, *Analytical Biochemistry*, 2011, **410**, 62-69.